Max-Planck-Institut
für Meteorologie

REPORT No. 240

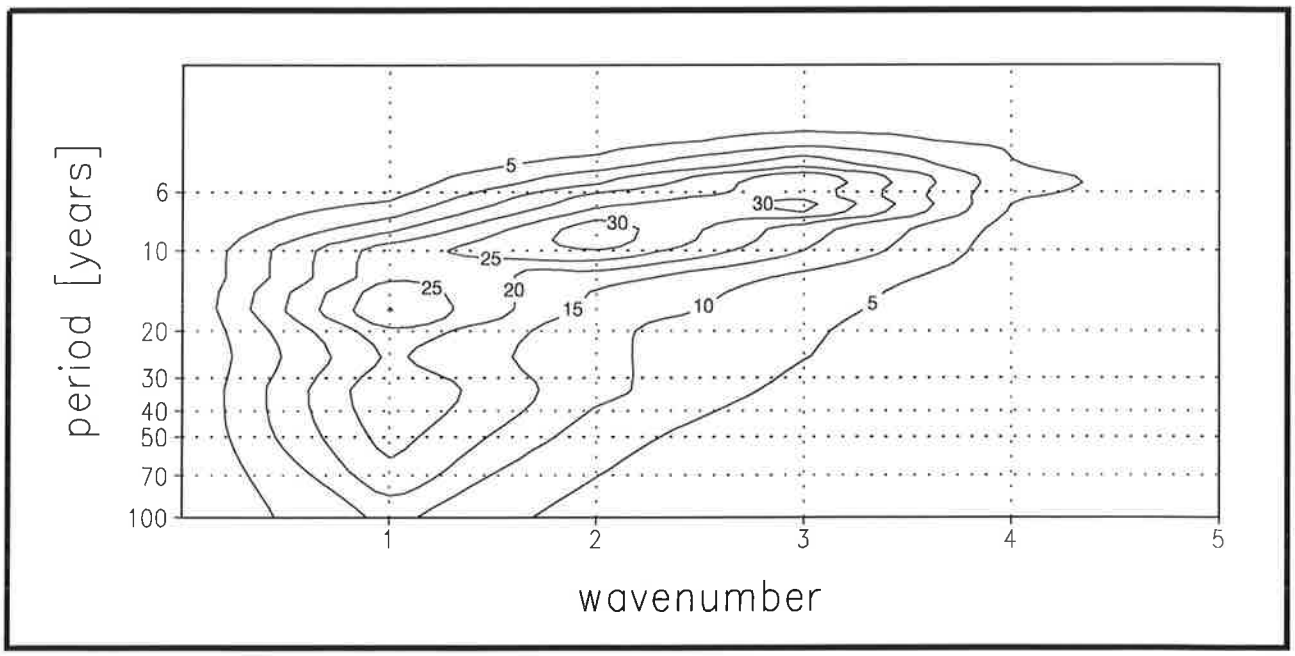

STOCHASTICALLY FORCED VARIABILITY IN THE ANTARCTIC CIRCUMPOLAR CURRENT

by

Ralf Weisse • Uwe Mikolajewicz
Andreas Sterl • Sybren S. Drijfhout

HAMBURG, August 1997

AUTHORS:

Ralf Weisse

GKSS
Institut für Gewässerphysik
Max-Planck-Str. 1
D-21502 Geesthacht
Germany

Uwe Mikolajewicz

Max-Planck-Institut
für Meteorologie
Bundesstr. 55
D-20146 Hamburg
Germany

Andreas Sterl
Sybren S. Drijfhout

Koninklijk Nederlands Meteorologisch Instituut
Postbus 201
NL-3730 AE De Bilt
The Netherlands

MAX-PLANCK-INSTITUT
FÜR METEOROLOGIE
BUNDESSTRASSE 55
D - 20146 HAMBURG
GERMANY

Tel.: +49-(0)40-4 11 73-0
Telefax: +49-(0)40-4 11 73-298
E-Mail: <name> @ dkrz.de

Stochastically forced variability in the Antarctic Circumpolar Current

Ralf Weisse

Max-Planck-Institut für Meteorologie, Hamburg, Germany

(present affiliation: GKSS Institut für Gewässerphysik, Geesthacht, Germany)

Uwe Mikolajewicz

Max-Planck-Institut für Meteorologie, Hamburg, Germany

Andreas Sterl

Koninklijk Nederlands Meteorologisch Instituut, De Bilt, The Netherlands

Sybren S. Drijfhout

Koninklijk Nederlands Meteorologisch Instituut, De Bilt, The Netherlands

Submitted to Journal of Geophysical Research

July 31, 1997

ISSN 0937 - 1060

Correspondance: weisse@gkss.de

Abstract

Decadal fluctuations in the Antarctic Circumpolar Current (ACC) were considered. Recently, the concept of the Antarctic Circumpolar Wave was proposed to account for large-scale anomalies which tend to propagate along the ACC in both the atmosphere and the ocean. In the present study the Hamburg Large-Scale Geostrophic ocean general circulation model was forced stochastically to assess whether such anomalies can partially be explained by a simple ocean response to atmospheric forcing. The short-term atmospheric weather fluctuations were represented by a number of spatially coherent patterns of momentum, heat, and freshwater flux which were superimposed onto the climatological fluxes. These patterns were derived from an experiment with an atmospheric general circulation model forced with observed sea surface temperatures and were chosen randomly at each time step of the ocean model. We found that in this experiment anomalies which propagate along the ACC on a decadal time scale occur and that they can be explained by the combined effects of anomaly advection with the mean ocean circulation and integration of the short-term atmospheric weather fluctuations. In this case, the spatial scale of the anomalies as given by the atmosphere is converted into a time scale by the mean zonal velocity of the ACC.

1. Introduction

Almost unaffected by continental barriers the Antarctic Circumpolar Current (ACC) encircles the globe and forms one of the largest current systems of the world oceans. By connecting the Pacific, the Atlantic, and the Indian Ocean the ACC enables the exchange of water masses between these three major ocean basins, and plays an important role within the global ocean circulation. The ACC forms the northern boundary for the Southern Ocean which represents an important component of the climate system. Antarctic bottom water, one of the coldest and densest water masses, is formed in the Southern Ocean. It is this water mass which cools and ventilates most of the volume of the deep oceans (e.g. Schmitz, 1995).

There is considerable interannual and decadal variability at high southern latitudes, and observations of sea-ice extent suggest that these features tend to propagate along the ACC (e.g. Lemke et al., 1980; Murphy et al., 1995). Phase-locked anomalies of sea surface temperature (SST), sea-ice extent, sea level pressure (SLP) and meridional wind stress propagating eastward along the ACC were described by White and Peterson (hereafter WP) (1996). They suggested that the anomalies circle around Antarctica in roughly 8-10 years at an average speed of

6-8 cms^{-1}. Since a wavenumber two like pattern was most dominant in their data a time scale of 4-5 years was deduced. WP called this phenomenon the Antarctic Circumpolar Wave (ACW). The ACW was also identified by Jacobs and Mitchell (1996) in variations of the sea surface height in the ACC using the most recent satellite data available.

Peterson and White (hereafter PW) (1996) suggested that the ACW basically reflects a propagation of Pacific ENSO signals and that the source for the interannual SST signals in the ACC is located in the western subtropical South Pacific ocean. They concluded that ENSO-related SST anomalies propagate southward into the Southern Ocean where they move eastward, phase-locked with SLP anomalies, around the entire southern hemisphere through some combination of geostrophic advection and ocean-atmosphere coupling.

With respect to the time scale considered the period for which reliable data are available at high southern latitudes is rather limited. The validity of some of WP's and PW's conclusions must therefore be considered with care. Christoph et al. (hereafter CBR) (1997) tried to find and confirm WP's and PW's results in a 180-year integration of a coupled atmosphere-ocean general circulation model (CGCM). They found variability strongly reminiscent of the ACW but raised some noticeable differences. In the model the turn-around time of the ACC is closer to 12-16 years compared to the 8-10 years inferred from the observations and a wavenumber three pattern is more pronounced than a wavenumber two pattern. Additionally, CBR (1997) found noticeable regional differences in the amplitude of the ACW-like variability which is much smaller in the South Atlantic and Southern Indian Ocean than in the Pacific. Based on these findings they doubted that the ACW indeed circles around the globe, and concluded that an equally plausible description would have the ACW appear first south of Australia, subsequently moving eastward with intensification, and immediately attenuating after passing Drake Passage. Whereas PW speculated that the ACW has its source in the ENSO phenomenon CBR (1997) argued that the mode has its origins in the mid- to high latitudes themselves.

Both, WP (1996) and CBR (1997) concluded that the ACW is a mode of the coupled atmosphere ocean sea-ice system and that atmosphere-ocean interaction plays a dominant role in the mechanism of the variability. This is a typical approach often used to explain variability of the type described above. An alternative attempt at understanding climate variability was proposed by Hasselmann (1976) with the concept of stochastic climate models. For time scales of a few months and longer the atmosphere is assumed to be in a quasi-equilibrium. The integration of the short-term atmospheric fluctuations transforms the essentially white-noise atmos-

pheric forcing into a red response signal. For a linear system the resulting response spectrum is proportional to ω^{-2} as long as the frequency ω is large compared to the inverse of the natural time scale of the slow system and constant at low frequencies. This concept was successfully applied to a number of problems such as mid-latitude SST variability (Frankignoul and Reynolds, 1983) or advection of sea-ice in the Arctic and Antarctic (Lemke et al., 1980). Note, however, that ocean-atmosphere feedbacks are usually neglected in simple linear stochastic climate models.

The purpose of the present paper is to investigate to what extent the concept of stochastic climate models can be applied to explain decadal climate variability in the Southern Ocean. For that purpose we forced a stand-alone ocean general circulation model (OGCM) with stochastic wind stresses, heat and freshwater fluxes superimposed on the climatological fluxes and integrated the model for 5000 years. In this way a strong decadal signal was excited in the Southern Ocean which shows substantial similarities with the ACW. This signal can be understood as the oceanic response to the white-noise atmospheric forcing and can be explained mainly by an integration of the stochastic components of the atmospheric forcing plus ocean advection and some linear ocean feedback. Atmospheric feedbacks are neglected in our study.

The OGCM and the experiment are briefly described in Section 2. The ACW as it appears in the OGCM is described in Section 3.1 Based on the concept of stochastic climate models a simple physical model for the decadal variability in the ACC is presented and tested against the OGCM results in Section 3.2 and 3.3. Regional differences in the role of advection are considered in section 3.4. Our results are summarized and discussed in Section 4.

2. Model and experiment description

2.1. The model and the spin-up

In the present study the Hamburg Large-Scale Geostrophic (LSG) OGCM as described by Maier-Reimer et al. (1993) was used. The model is based on the linearized Navier-Stokes equations, the conservation equations for heat and salt and the equations of state (UNESCO, 1983) and continuity. In the latter, incompressibility is assumed. In case of static instability convective adjustment is applied. The model has a free upper surface. A mass flux boundary condition is used at the sea surface. A simple sea-ice model is included in which sea-ice is advected by the ocean mean surface velocity as well as by wind with an assumed equilibrium

velocity proportional to the wind velocity. Furthermore, a simple run-off model is included.

The LSG OGCM is formulated on an Arakawa E-Grid (Arakawa and Lamb, 1977) and, in the present study, was applied with a horizontal resolution of effectively 3.5^{o}x3.5^{o} at 11 vertical levels, centered at 25, 75, 150, 250, 450, 700, 1000, 2000, 3000, 4000 and 5000 m. A realistic but smoothed topography was used and a time step of 15 days was applied.

A model spin-up was performed for 5000 years using monthly climatologies of COADS near-surface air temperature (Woodruff et al., 1987), wind stress (Hellerman and Rosenstein, 1983) and annual mean climatologies of sea surface salinities (Levitus, 1982) until a steady-state solution was obtained. Climatologies of net freshwater flux and heat flux were computed from the last 500 years of this spin-up. The model was integrated for another 4000 years using a fixed flux boundary condition for freshwater flux and a combination of a fixed flux forcing and restoring with a damping coefficient of 16 $Wm^{-2}K^{-1}$ as boundary condition for temperature (Mikolajewicz and Maier-Reimer, 1994).

2.2. Description of the experiments

To account for the short-term atmospheric fluctuations which influence the ocean at its upper boundary stochastic components were added to the climatological fluxes of momentum, fresh-water and heat. These components were derived from a 10-year AMIP simulation with the ECHAM3-T42 AGCM (Arpe et al., 1993) by averaging the momentum, heat and freshwater fluxes and the near-surface air temperature over each month and subtracting the climatology. For each month, one set of these anomalies was chosen at random and added to the climatological fluxes in the OGCM simulation. To account for the differences in the variability of the summer and the winter season, only anomalies from the corresponding month of the atmospheric simulation were chosen. Thus, the stochastic components superimposed are spatially coherent, but have a white-noise spectrum with respect to time. In the absence of reliable and sufficiently resolved observational data this spatial coherence may be regarded as a reasonable approximation for representing the spatial coherence at the synoptic scale of the atmosphere. The model was integrated for 7000 years. However, only the last 5000 years were examined in the present study to avoid analyzing of effects of the model's adaption to the new boundary conditions.

3. Decadal variability in the Antarctic Circumpolar Current

3.1. Analysis and description

To describe the space-time dependent variability appearing in the OGCM we used the multivariate Principal Oscillation Pattern (POP) technique (e.g. von Storch et al., 1995). In contrast to the Empirical Orthogonal Function (EOF) analysis which is designed to yield an optimal representation of the covariance structure in the data and not to represent dynamical modes in general the POP analysis provides a simultaneous analysis of both the spatial features (e.g. propagation) and the spectral characteristics of the data. Examples of the good agreement between the theoretical normal modes of a complex system and those estimated by a POP analysis can be found in Schnur et al. (1993).

POP's form an eigensystem of the analyzed data $\boldsymbol{y}(\boldsymbol{x}, t)$

$$\boldsymbol{y}(\boldsymbol{x}, t) = \sum_i z_i(t)\boldsymbol{p}_i(\boldsymbol{x}), \tag{1}$$

where $z_i = z_{i1} + iz_{i2}$ are the complex POP coefficient time series and $\boldsymbol{p}_i = \boldsymbol{p}_{i1} + i\boldsymbol{p}_{i2}$ are the spatial POP patterns. Vectors are typed in boldface. The system is expected to generate stochastic sequences

$$\ldots \rightarrow \boldsymbol{p}_2 \rightarrow \boldsymbol{p}_1 \rightarrow -\boldsymbol{p}_2 \rightarrow -\boldsymbol{p}_1 \rightarrow \boldsymbol{p}_2 \rightarrow \ldots. \tag{2}$$

Note that the index i was dropped for convenience. Thus, if at time $t=0$ the system is in state $\boldsymbol{p}_2$, it will be with a high probability in state $\boldsymbol{p}_1$ one quarter of a period later, in state $-\boldsymbol{p}_2$ half a period later, and so on.

We performed a POP analysis for the sea surface salinity (SSS) of the Southern Hemisphere in the LSG experiment. The dominant mode of variability (Figure 1) is characterized by an oscillation period of roughly 6 years. According to (2) it describes the eastward propagation of salinity anomalies along the ACC. The amplitude of the mode is at maximum in the Pacific sector (roughly 0.15 psu southeast of New Zealand), and almost negligible in the Indian Ocean. If we consider for example the positive salinity anomaly southwest of Australia (Figure 1a); the anomaly moves eastward under intensification first (Figure 1b), reaches maximum amplitude east of the dateline, and attenuates henceforth. There are clear indications of a zonal wavenumber three pattern, however, zonal modifications of the amplitude suggest that the

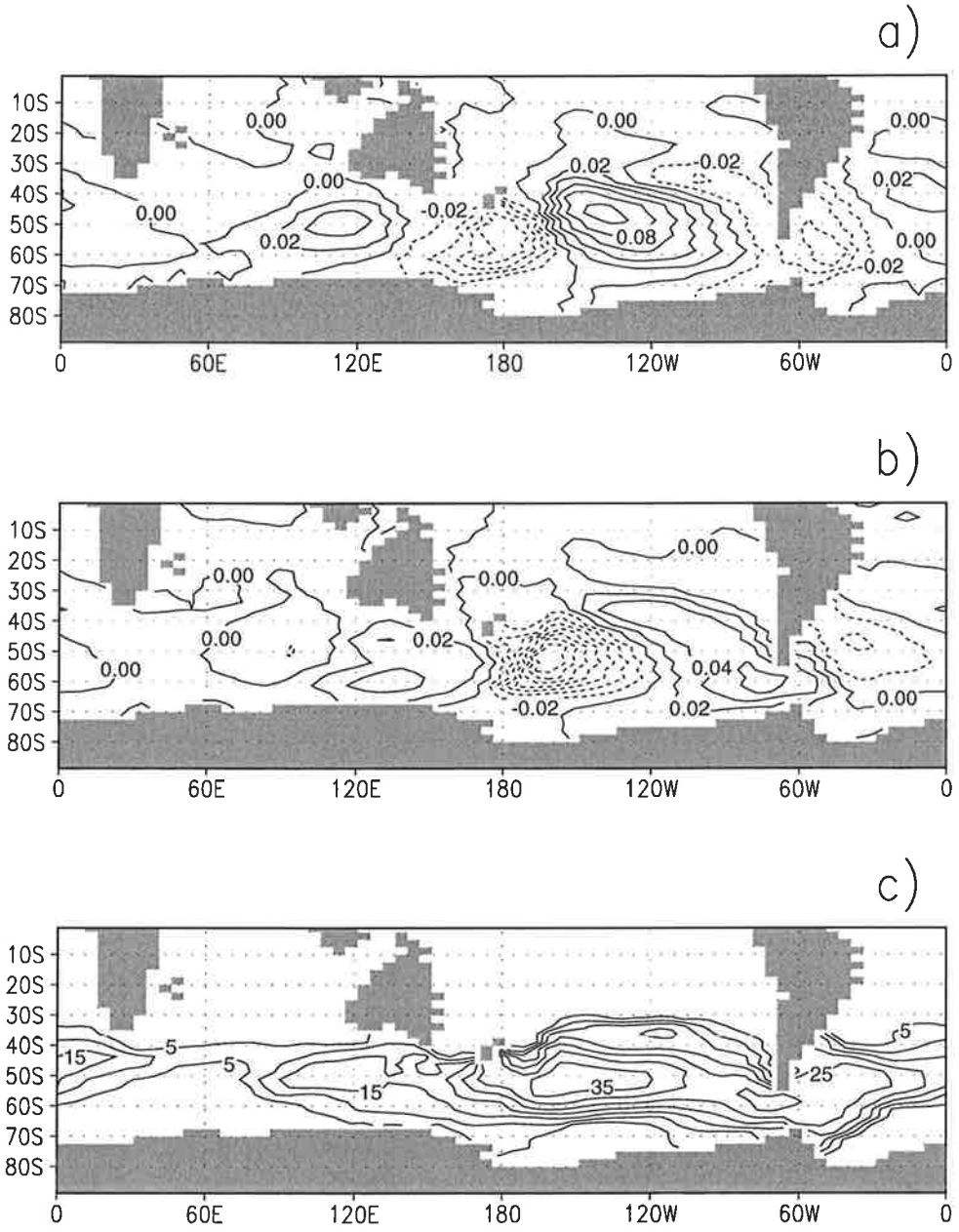

Figure 1. Spatial patterns of SSS in practical salinity units [psu] of the dominant mode of decadal variability in the Southern Ocean, (a) imaginary part, (b) real part and (c) locally explained variance. Contour interval is 0.02 psu for imaginary and real part (a,b) and 5% for locally explained variance (c). The model topography is indicated in grey. Note that the model is formulated on an Arakawa E-grid and that data and topography were transferred to a regular grid for plotting.

mode must be a combination of more than only one wavenumber. The mode explains up to 35 % of the model's total SSS variability in the ACC (Figure 1c). Locally, the explained variance is highest in the Pacific sector. The cross-spectra of the POP coefficient time series are characterized by a pronounced peak near the POP period (6 years), strong coherence, and a constant phase shift of roughly 90^{o} (Figure 2).

Local values for growth and decay rates can be deduced from the relative locations and the absolute values of the POP maxima and minima (Schnur, 1993). A schematic sketch of the POP is shown in Figure 3. Three different regions can be characterized. Southwest of Australia and New Zealand, the POP describes a growth of anomalies with an increasing rate from west to east. In the region from 160^{o} West to east of Drake Passage the amplitude of the POP decreases, while near Drake Passage the decay is temporally halted. In the Indian Ocean the amplitudes are negligible. If we neglect the damping which is given by the relative strength of the imaginary and the real part of the POP coefficient time series and assume exponential decay and growth we can estimate an e-growth rate of roughly 2.2 years for the West Pacific and an e-folding time of roughly 2.9 years for the East Pacific sector..

Associated patterns $\boldsymbol{p}_A$ of temperature and salinity at the uppermost 4 levels (25, 75, 150, 250 metres depth) were computed for this POP to test if the mode exists in other parameters than SSS. Associated patterns evolve in phase with the estimated POP pattern (Figure 1) and are defined by

$$\left\| \boldsymbol{y}(\boldsymbol{x}, t) - z(t)\boldsymbol{p}_A(\boldsymbol{x}) \right\|^2 = Min, \tag{3}$$

where $\boldsymbol{y}(\boldsymbol{x}, t)$ represents the vector time series of temperature and salinity at the uppermost 4 levels and $z(t)$ denotes the complex POP coefficient time series. The associated pattern for temperature at 75 m depth describes an eastward propagating wavenumber three signal which accounts for roughly 20% of the local variance in the Pacific sector of the ACC (Figure 4). Similar results were found for temperature at 150 and 250 m depth. The amplitudes of the anomalies are approximately 0.2 K at 150 m, and 0.15 K at 250 m depth (not shown). Although anomalies in the associated patterns grow up to 0.35 K at the sea surface southeast of New Zealand, the signal-to-noise ratio is smaller at the sea surface due to the strong damping by the ocean-atmosphere heat fluxes. The situation is slightly different for the salinities. Here the signal is more confined to the upper two layers. At 250 m depth anomalies of signifi-

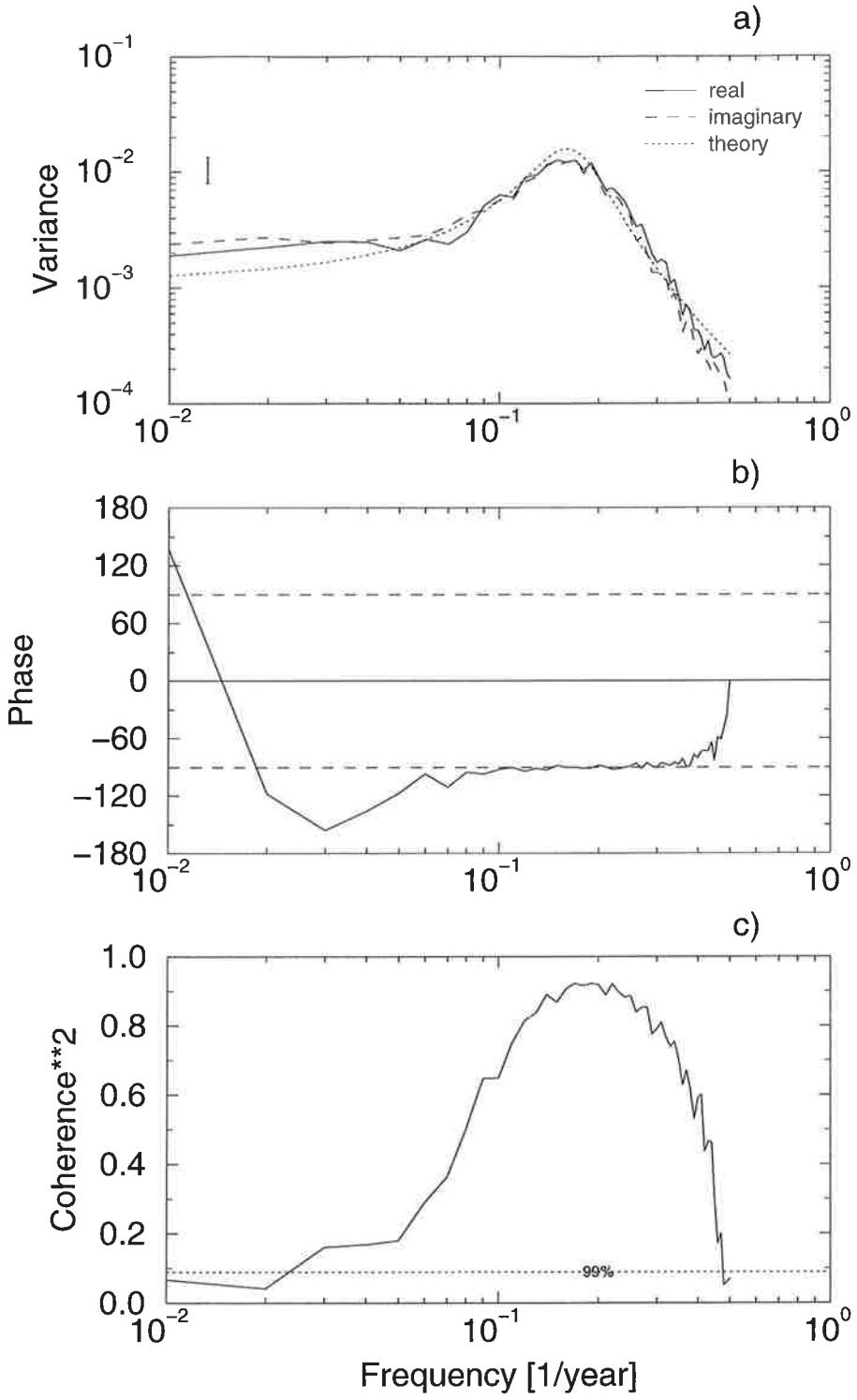

Figure 2. Spectra of the POP coefficient time series of the dominant mode of decadal variability in the ACC, (a) power spectrum (solid line, real component; dashed line, imaginary component; dotted line, fitted theoretical model; The bar on the left hand side represents the 95% confidence interval.), (b) phase spectrum, and (c) coherence squared.

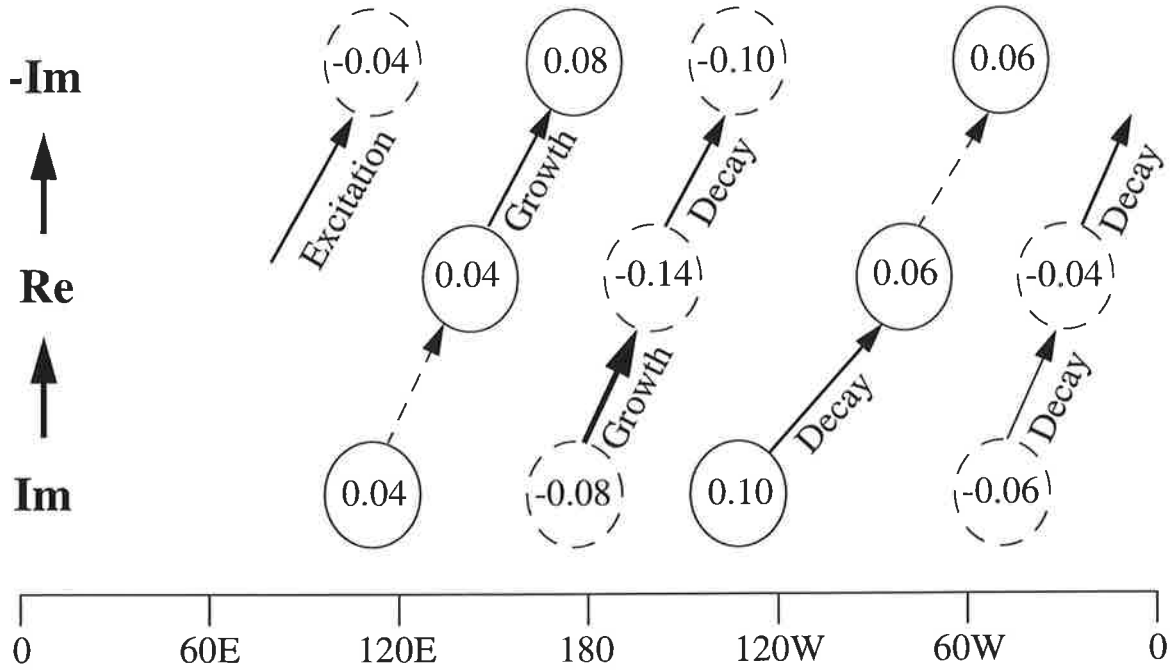

Figure 3. Schematic sketch of the dominant mode of decadal variability. Numbers denote the maximum amplitudes of positive (solid) and negative (dashed) anomalies. The width of the arrows shows qualitatively the growth and the decay rates (open) for the transition from the imaginary to the real and from the real to the negative of the imaginary part.

cant amplitude were only found southeast of New Zealand and account for roughly 25% of the local salinity variability. The confinement of the signal to a very limited region at deeper layers is probably due to the fact that anomalies here are induced by modified convection produced by the propagating surface anomalies.

The decadal variability described is to a large extent characterized by the eastward propagation of temperature and salinity anomalies. The path which the maxima of the anomalies follow coincides well with the trajectory of an imaginary passive tracer in the mean current. We therefore propose that the propagation of the anomalies is basically a result of ocean advection. On the other hand, the generation of the anomalies is probably mainly a result of the integration of the stochastic atmospheric forcing, and that the decadal variability found in the LSG

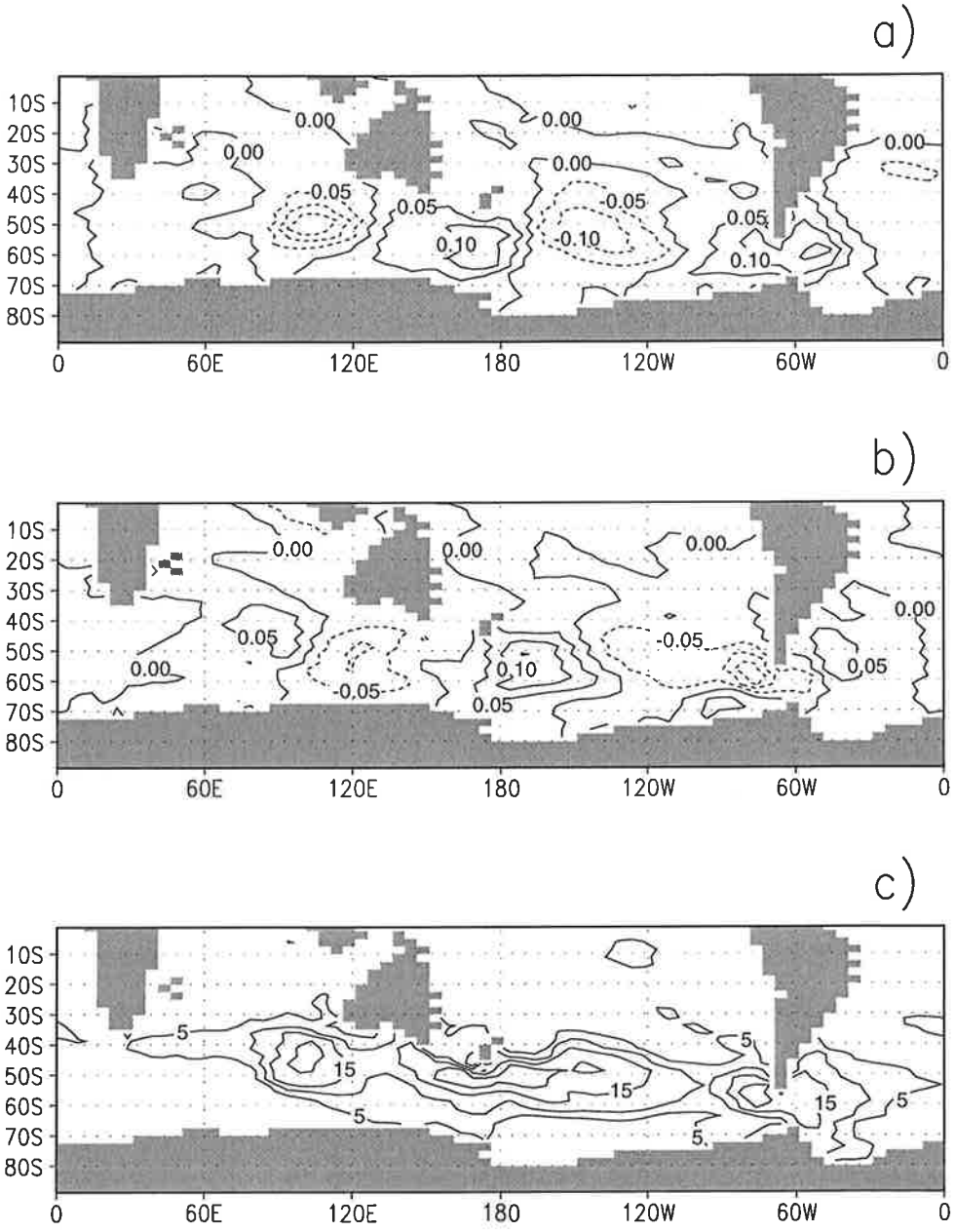

Figure 4. Associated patterns of the temperature in Kelvin [K] at 75 m depth, (a) imaginary part, (b) real part and (c) locally explained variance. Contour interval is 0.05 K for imaginary and real part (a,b) and 5% for locally explained variance (c). The model topography is indicated in grey. Note that the model is formulated on an Arakawa E-grid and that data and topography were transferred to a regular grid for plotting.

model can to a large extent be described as a combination of the integration of the white-noise atmospheric forcing, ocean advection, and some linear feedback. Based on this hypothesis a simple physical model for the oceanic variability is developed in Section 3.2 and compared to the results of the LSG experiment in Section 3.3.

3.2. A physical model

Consider the general transport equation for any property $y(x, t)$ like temperature or salinity

$$\frac{\partial y}{\partial t} + \nabla(uy) = s, \tag{4}$$

where $u(x, t)$ denotes velocity and $s(x, t)$ any source or sink of property y. The source term includes the atmosphere-ocean fluxes and, since we only consider the horizontal equation, fluxes from below such as, for instance, the flux due to convection. Thus, s is a function of oceanic and atmospheric variables. By averaging over a time period intermediate between the short time scale of the atmospheric fluctuations and the longer time scale of the ocean variability it can be divided into a mean component $\bar{s}$ depending on the ocean conditions, and a fluctuating part s' which describes the influence of the atmospheric short-term fluctuations:

$$s = \bar{s} + s' \tag{5}$$

For small perturbations around an equilibrium state we assume that $\bar{s}$ can be written as $\bar{s} = -\lambda y$ where λ is a constant (linear feedback) so that the transport equation (4) yields

$$\frac{\partial y}{\partial t} + \nabla(uy) + \lambda y = s'. \tag{6}$$

Equation (6) is formally similar to a stochastic climate model with linear feedback and advection in which the variability of the slowly varying oceanic variable is completely a result of the atmospheric noise forcing. Similar models were proposed and successfully applied to mid-latitude SST anomalies (Frankignoul and Reynolds, 1983) and to advection of sea-ice in the Arctic and Antarctic (Lemke et al., 1980).

For simplicity we consider only variations in the longitudinal direction in a surface layer of constant depth and approximate u by the mean zonal velocity of the ACC, independent of space and time. Then (6) becomes

$$\frac{\partial}{\partial t}y(x,t) + \bar{u} \bullet \frac{\partial y}{\partial x}(x,t) + \lambda y(x,t) = \nu(x,t), \tag{7}$$

where x denotes the longitude and $\nu = s'$. If we denote the space-time Fourier transformation by

$$\hat{y}(\omega, k) = \iint y(x,t) e^{-i(\omega t - kx)} dx dt, \tag{8}$$

where ω is the frequency and k is the zonal wavenumber, equation (7) can be written as

$$-i\omega\hat{y} + ik\bar{u}\hat{y} + \lambda\hat{y} = \hat{\nu}. \tag{9}$$

Multiplying (9) by its complex conjugate and ensemble averaging yields a relation between the wavenumber-frequency spectra of the atmospheric forcing and the oceanic response:

$$F_{yy}(\omega, k) = \frac{F_{\nu\nu}(\omega, k)}{(\omega - k\bar{u})^2 + \lambda^2}, \tag{10}$$

where F_{ab} denotes the cross spectrum between a and b. It can be inferred from (10) that for a white-noise atmospheric forcing the wavenumber-frequency spectrum of the ocean response F_{yy} has a maximum at $\omega_0 = k_0\bar{u}$ for each wavenumber k_0. In other words, in the wavenumber-frequency domain F_{yy} peaks along lines of constant ωk^{-1}.

The variance spectrum can also be expressed in terms of the wavenumber-frequency spectrum:

$$F_{yy}(\omega) = \int \frac{F_{\nu\nu}(\omega, k)}{(\omega - k\bar{u})^2 + \lambda^2} dk. \tag{11}$$

If the atmospheric forcing is white in time $F_{\nu\nu}(\omega, k)$ reduces to $F_{\nu\nu}(0, k)$. From (11), it can be inferred that the variance spectrum is not necessarily peaked, but depends on the shape of the spectrum of the forcing. If, for instance, the spectrum of the forcing is almost constant with respect to frequency but has a distinct maximum at wavenumber k_0, the variance spectrum will have a peak at the frequency $k_0\bar{u}$. In this case, it is the spatial coherence of the forcing which is mapped onto the slow system and determines the time scale of the ocean response.

3.3. Model testing

To check the consistency between the variability found in the LSG and the simple model proposed in the previous section we computed the wavenumber-frequency spectra of SSS and temperature at 75 m depth at 51° and 61° South from the LSG experiment data and compared them with the spectrum (10) of the physical model. Hence, temperature and salinity were expanded into a series of sine and cosine functions along each latitude belt. The bivariate time series, composed of the time dependent sine and cosine coefficients ($b_k(t)$ and $a_k(t)$), is assumed to be a random realization of a bivariate stochastic process and is used to estimate the wavenumber-frequency spectrum given by

$$F_{ab}(\omega, k) = \frac{1}{2}[F_{aa} + F_{bb}](\omega) - Q_{ab}(\omega), \tag{12}$$

where Q_{ab} represents the quadrature-spectrum of the sine and cosine coefficients (von Storch and Zwiers, 1997). Additional heuristic arguments are used to assign parts of the overall variance to standing and propagating waves. We used the definition of Pratt (1976) who interprets the minimum of westward and eastward propagating variance as standing variance and labels the remainder as propagating variance. With this interpretation, the standing variance comprises all standing plus all random fluctuations.

A large fraction of the SSS variance at 51° South is accounted for by a standing wavenumber one pattern with a 40-50 year time scale (Figure 5b). Near the POP period, most of the SSS variance is attributed to the propagating part of the spectrum at zonal wavenumbers 1-3 (Figure 5a). In accordance with the spectrum of the proposed simple model (10) the maximum of the propagating variance is centered along a line of almost constant $k\omega^{-1}$. For $k=1$, the maximum variance occurs at a period of roughly 18 years, for $k=2$ at roughly 9 years, and for $k=3$ at roughly 6 years, resulting in a propagation speed of 20° per year or 4.5 cms^{-1} at 50° South which coincides with the speed of the ACC in the LSG model. The wavenumber-frequency spectrum of temperature at 75 m depth looks similar to that of SSS, however with a smaller signal-to-noise ratio (not shown). For both temperature and salinity, the wavenumber-frequency spectra were found to be similar to that of the simple model (10).

To test the hypothesis that the spatial patterns of the atmosphere are dominated by only a few wavenumbers and thereby might determine the time scale of the ocean response we computed

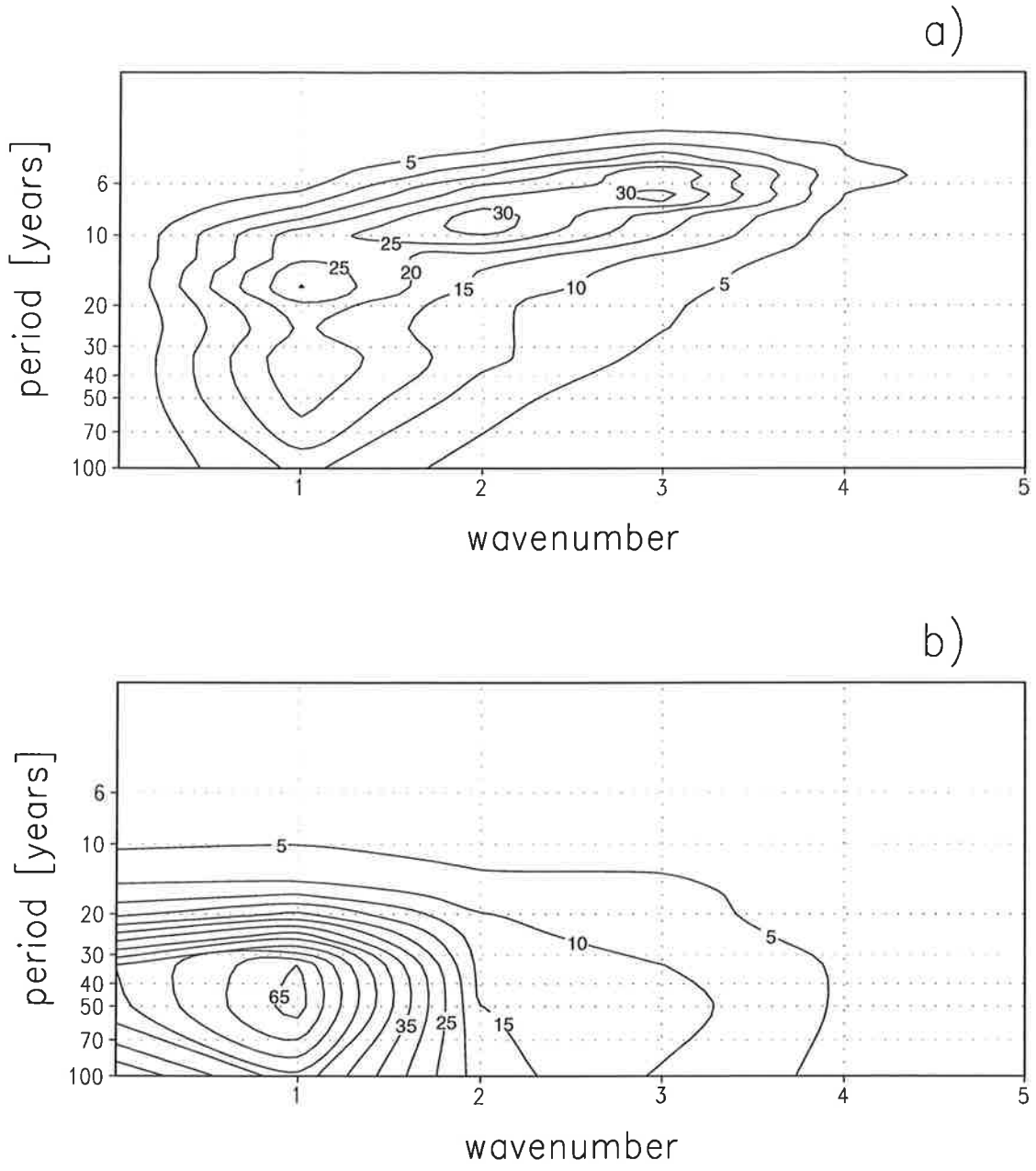

Figure 5. Two-sided wavenumber-frequency spectrum of the SSS at 51° South in 10^{-5} psu$^2\Delta\omega^{-1}\Delta k^{-1}$, (a) propagating variance and (b) standing variance.

the wavenumber-frequency spectra of all atmospheric forcing components (boundary temperature, net freshwater flux, and wind stress curl) in the LSG experiment (Figure 6). The terminology "atmospheric forcing" should be interpreted here in the formal sense, as representative of the true forcing, the assumption being that the true forcing is significantly correlated with the chosen atmospheric variable. Most of the variance in these spectra is attributed to the large scale (wavenumbers 1-3). Assuming that the proposed model (7) holds, a combination of more than one dominant wavenumber in the forcing fields is necessary to account for the zonal modifications of the amplitude of the ocean response as found for the POP mode (Figure 1). With respect to frequency, the wavenumber-frequency spectra are almost constant which is typical for white-noise processes. The variance of the model forcing which is attributed to the standing part of the spectrum is usually one to two orders of magnitude larger than that associated with the propagating part. This results from the fact that the atmospheric forcing of the LSG experiment consists of a limited number of spatial patterns which were chosen randomly in time. Thus, there is no preferred propagation direction so that the variance is dominated by the standing part of the spectrum. Therefore, only the total variance is shown in Figure 6. Although we cannot draw any conclusions from the relative amount of atmospheric variance explained by the propagating and the standing part of the spectrum, there is some observational evidence that the chosen forcing nevertheless represents an adequate approximation of the real situation. For instance, Mo and White (1985) and Xu et al. (1990) report a preference of the atmosphere to attribute energy to the standing part of the spectrum in the mid-latitudes of the southern hemisphere.

For simplicity, we assume that the white-noise atmospheric forcing $F_{vv}(\omega, k)$ is dominated by a wavenumber three pattern. Then (11) reduces to

$$F_{TT}(\omega) = \frac{A_{vv}}{(\omega - 3\bar{u})^2 + \lambda^2} \tag{13}$$

where $A_{vv} = F_{vv}(\omega, k)$ is the constant amplitude of the stochastic forcing. We fitted the spectrum of the simple physical model (13) to the spectrum of the POP coefficient time series and obtained a good agreement between the theoretical spectrum (13) and that derived from the POP coefficient time series (Figure 2). The model parameters A_{vv}, $\bar{u}$, and λ were estimated by a least squares fit, minimizing the deviation between the power spectra of the POP coefficients and the advective model. The least squares solution was obtained using a simu-

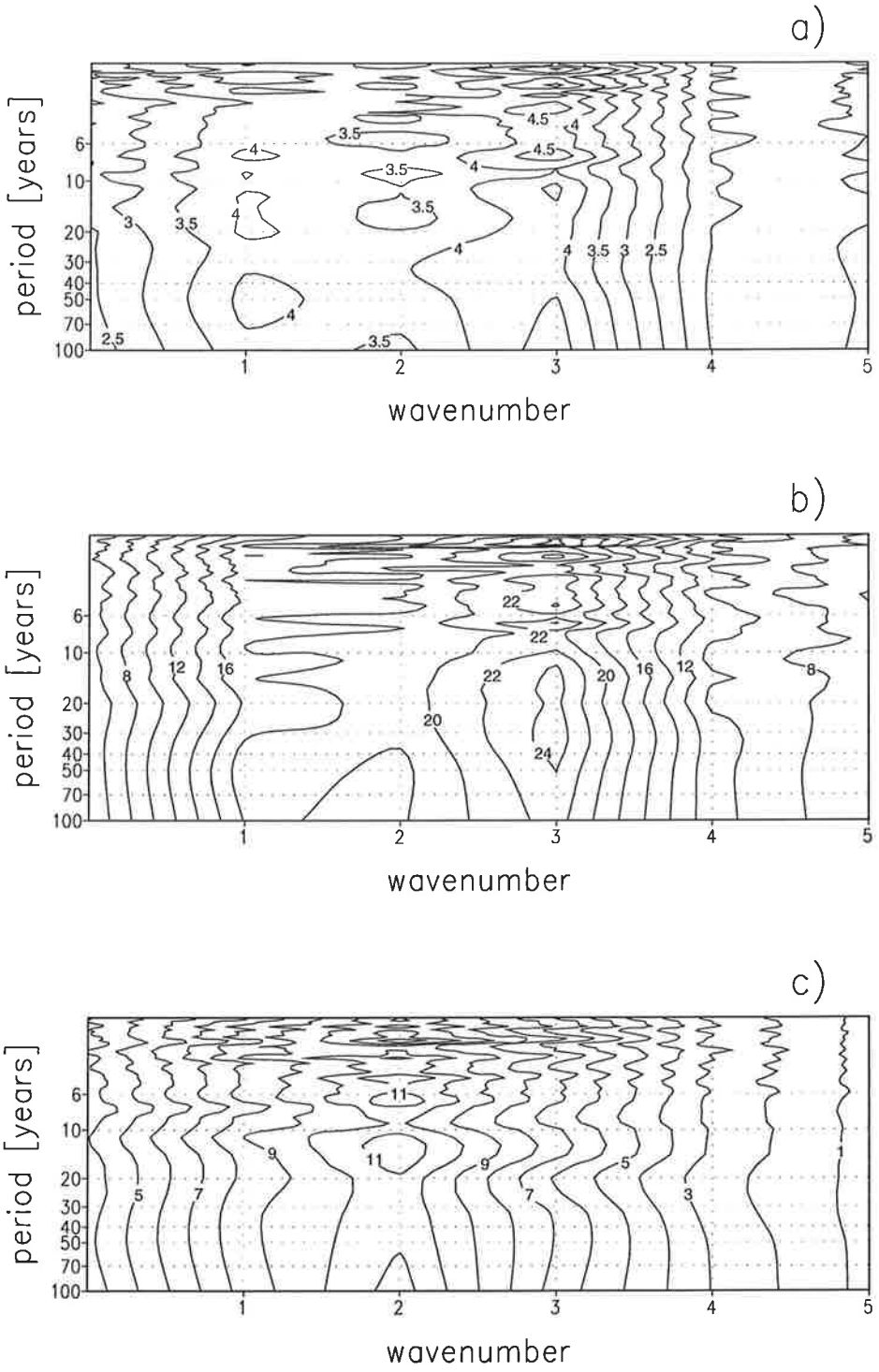

Figure 6. One-sided wavenumber-frequency spectra of the atmospheric forcing at 51° South, (a) wind stress curl in $10^{-12}\mathrm{Pa}^2\mathrm{m}^{-2}\Delta\omega^{-1}\Delta k^{-1}$, (b) net freshwater flux in 10^{-2} $(\mathrm{mm/month})^2\Delta\omega^{-1}\Delta k^{-1}$ and (c) boundary temperature in 10^{-5} $\mathrm{K}^2\Delta\omega^{-1}\Delta k^{-1}$.

lated annealing technique (e.g. Press et al., 1992). In this way we obtained a mean velocity $\bar{u}$ of roughly 0.34 rad per year, which is equivalent to almost 19° per year, or 4-5 cms^{-1} at 51° South. This coincides with the average speed of the ACC in the LSG model and yields a turn-around time around Antarctica of roughly 19 years. Because of the assumed wavenumber three pattern in the atmospheric forcing, this corresponds to a characteristic time scale of roughly 6 years which coincides with the estimated POP period. The feedback term λ yields 0.28 yr^{-1} which corresponds to an e-folding time of almost 4 years. The white-noise forcing level was estimated to be 1.239×10^{-3} yr^{-1}. Note that POP coefficient time series are dimensionless in our case.

To demonstrate the skill of the proposed model a one dimensional model for the surface temperature T at 51° South was constructed from (7):

$$\frac{T_{x,t+1}-T_{x,t}}{\Delta t}+\bar{u}\frac{T_{x+1,t}-T_{x,t}}{\Delta x}+\frac{\kappa}{c_p\rho\Delta z}T_{x,t}=\frac{\nu_{x,t}}{c_p\rho\Delta z} \tag{14}$$

and integrated forward in time for 100 years. Here, x denotes longitude, t time, $c_p = 3994$ $Jkg^{-1}K^{-1}$ the specific heat of sea water at constant pressure and $\rho = 1000$ kgm^{-3} the density of water. The ratio of the damping factor κ and the surface layer thickness Δz was chosen to be $3.6x10^{-2}$ $Wm^{-3}K^{-1}$ which corresponds to a linear feedback of $\lambda = 0.28$ $year^{-1}$ as estimated from the POP coefficients. The average velocity $\bar{u}$ was set to 4.5 cms^{-1}, the zonal resolution Δx to roughly 350 km which corresponds to 72 grid points at 51° South, and the time step to 1 month. The white-noise forcing function ν was represented as

$$\nu(x,t) = A_{\nu\nu}(t)\sin(kx) \tag{15}$$

where k denotes the dominant wavenumber of the forcing. The amplitude of the forcing $A_{\nu\nu}$ was chosen randomly with respect to time. Figure 7 shows Hovmoeller diagrams for $k = 3$ (a) and a superposition of wavenumbers 2 and 3 (b). In both cases, there are clear indications for anomalies propagating at the mean current velocity yielding a turn-around time of 18 years. If the variance of the forcing is dominated by only one wavenumber no zonal modi-

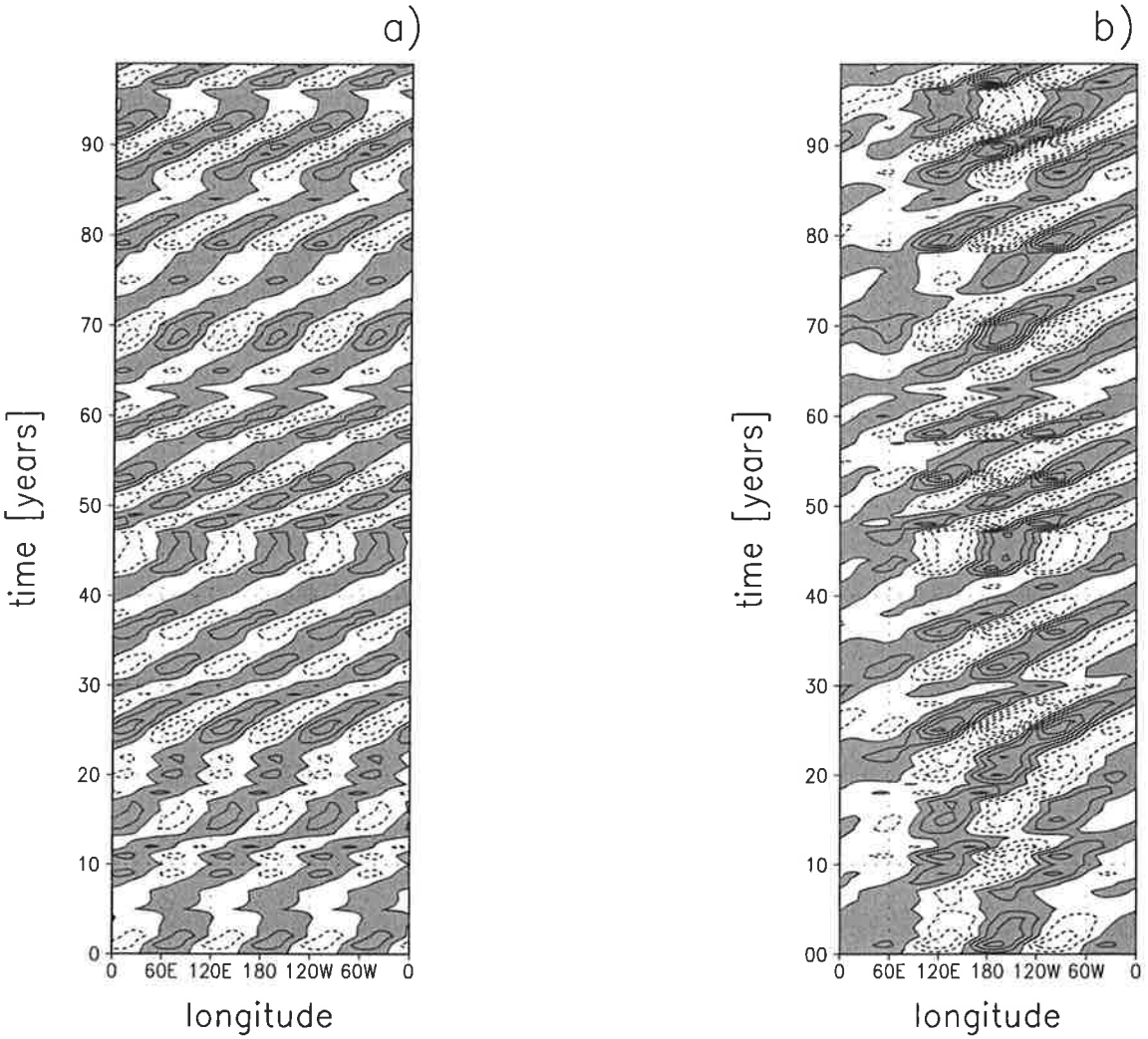

Figure 7. Hovmoeller diagrams of simulated SST response at 51° South using a simple 1-dimensional model of the ACC with randomly forced wavenumber 3 atmospheric patterns (a) and a superposition of randomly forced wavenumber 2 and 3 atmospheric patterns (b). Contour interval is 0.04 K. Isolines with negative values are dashed. Areas with positive values are shaded. Transition between white and grey area marks the zero line.

fications of the amplitude of the ocean response are found (Figure 7a). However, if it is a combination of at least 2 wavenumbers, remarkable zonal amplitude modifications are obtained. There is a noticeable agreement between the variability in the LSG model as described by the POP-mode and the results obtained with the proposed simple model (7). Note that the longitude is artificial in Figure 7.

3.4. Local role of advection

From the patterns of the POP mode and the locally explained variance (Figure 1) it can already be inferred that the mode is basically restricted to the Pacific sector of the ACC with excitation or strong enhancement of anomalies occurring southwest of Australia and New Zealand and attenuation occurring near Drake Passage. To confirm that this interpretation is supported by the raw data, we computed the cross correlation matrix $R_i(\tau, m)$ of the SSS at 51°S:

$$R_i(\tau, m) = \begin{cases} \frac{1}{N-\tau} \sum_{t=1}^{N-\tau} x(i+m, t+\tau)x(i, t) & , \tau > 0 \\ \frac{1}{N-|\tau|} \sum_{t=|\tau|+1}^{N} x(i+m, t-|\tau|)x(i, t)) & , \tau < 0 \end{cases} . \quad (16)$$

Here $x(i, t)$ denotes the SSS anomalies at longitude i and time t. $R_i(\tau, m)$ represents the cross correlation between grid points i and $i+m$ for time lag τ. N is the number of time steps.

The cross correlation plotted as function of i and m at given time lags indicates that advection of SSS anomalies plays an important role in the large-scale dynamics of the Southern Ocean (Figure 8). With increasing lags the maximum correlation is shifted from the center to the lower right triangle. Since positive lags indicate that the grid points on the ordinate lead the grid points on the abscissa and vice versa, a downstream propagation of the anomalies can be inferred from Figure 8.

To identify regions of excitation, extinction and almost pure advection we computed the spread s and the asymmetry a from the cross correlation matrix (16) by

$$s_i(|\tau|) = \frac{f_i(\tau) + f_i(-\tau)}{2} \quad (17)$$

$$a_i(|\tau|) = \frac{f_i(-\tau) - f_i(\tau)}{2}, \quad (18)$$

where

$$f_i(\tau) = max\{R_i(\tau, m), m = 1, M\}. \quad (19)$$

Here M denotes the number of grid points. Since the longitude m_0, at which the maximum

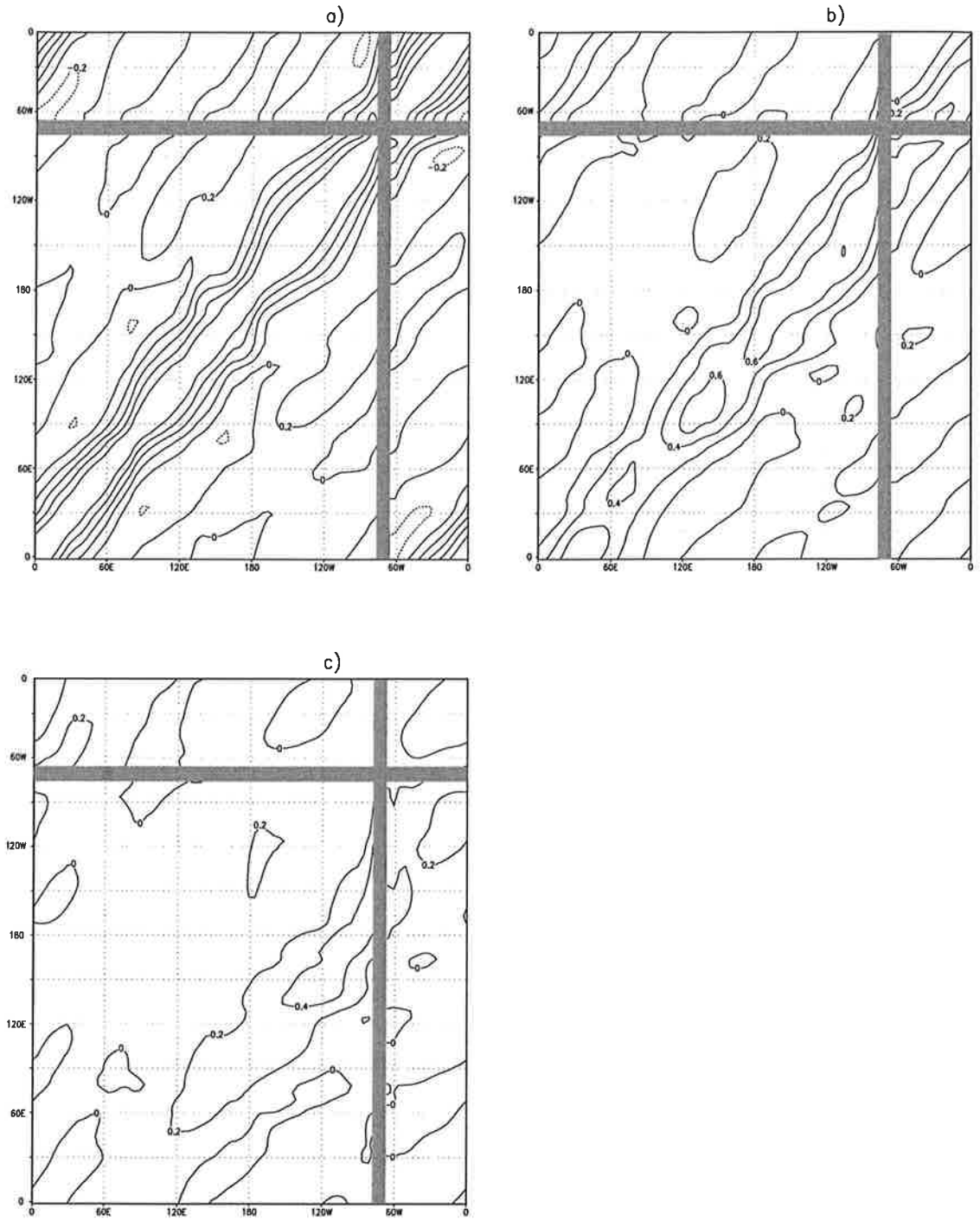

Figure 8. Cross-correlation matrix of SSS at 51° South for time lags of (a) 0 years, (b) +2 years and (c) +4 years. Contour interval is 0.2. Land points are shaded.

correlation $R_i(\tau, m_0)$ was found is always located downstream of the grid point i for $\tau > 0$ and upstream i for $\tau < 0$, asymmetry and spread can be interpreted in the following way: Small asymmetries, resulting from correlations of approximately the same magnitude up- and downstream, indicate that nearly pure advection is likely near point i, although other processes might result in small asymmetries as well. On the other hand, large asymmetries indicate that almost pure advection is unlikely to occur near point i. For the excitation of anomalies we would expect higher correlations downstream resulting in negative asymmetries, whereas extinction regions are given by positive asymmetries. The spread of the autocorrelation provides a measure of the internal memory of the system. The smaller the spread the smaller the memory and vice versa.

Spread and asymmetry as function of i and τ for salinity at 51° South are shown in Figure 9. The largest asymmetry is found at 95° East southwest of Australia. The minus sign indicates that the anomalies are excited here. The location of this large negative asymmetry coincides with the westernmost region in which noticeable amplitudes of the POP patterns can be found (Figure 1). Downstream of this region almost zero asymmetries indicate that nearly pure advection is found here, although there is some enforcement or weakening of the anomalies superimposed at some places. Strongest extinction of salinity anomalies can be found near 30° East and around Drake Passage. The latter is probably a combination of disappearing and of splitting of the anomalies; parts of it move northeastward along the American west coast, parts of it are squeezing through Drake Passage and are disappearing in the Atlantic sector.

The spread is small in the East Atlantic and the Indian Ocean and at maximum in the Pacific sector. Since the spread is an indicator of the internal memory of the system these zonal modifications suggest that zonal variations of the linear feedback parameter λ do exist. Relative to advection local damping is thus stronger in the Indian Ocean and the East Atlantic and advection is more important in the Pacific sector.

4. Summary and discussion

The Hamburg LSG OGCM was forced with stochastic components added to the climatological fluxes of momentum, heat, and freshwater. Thereby, pronounced decadal variability in the Southern Ocean was excited. It is characterized by salinity and temperature anomalies in the

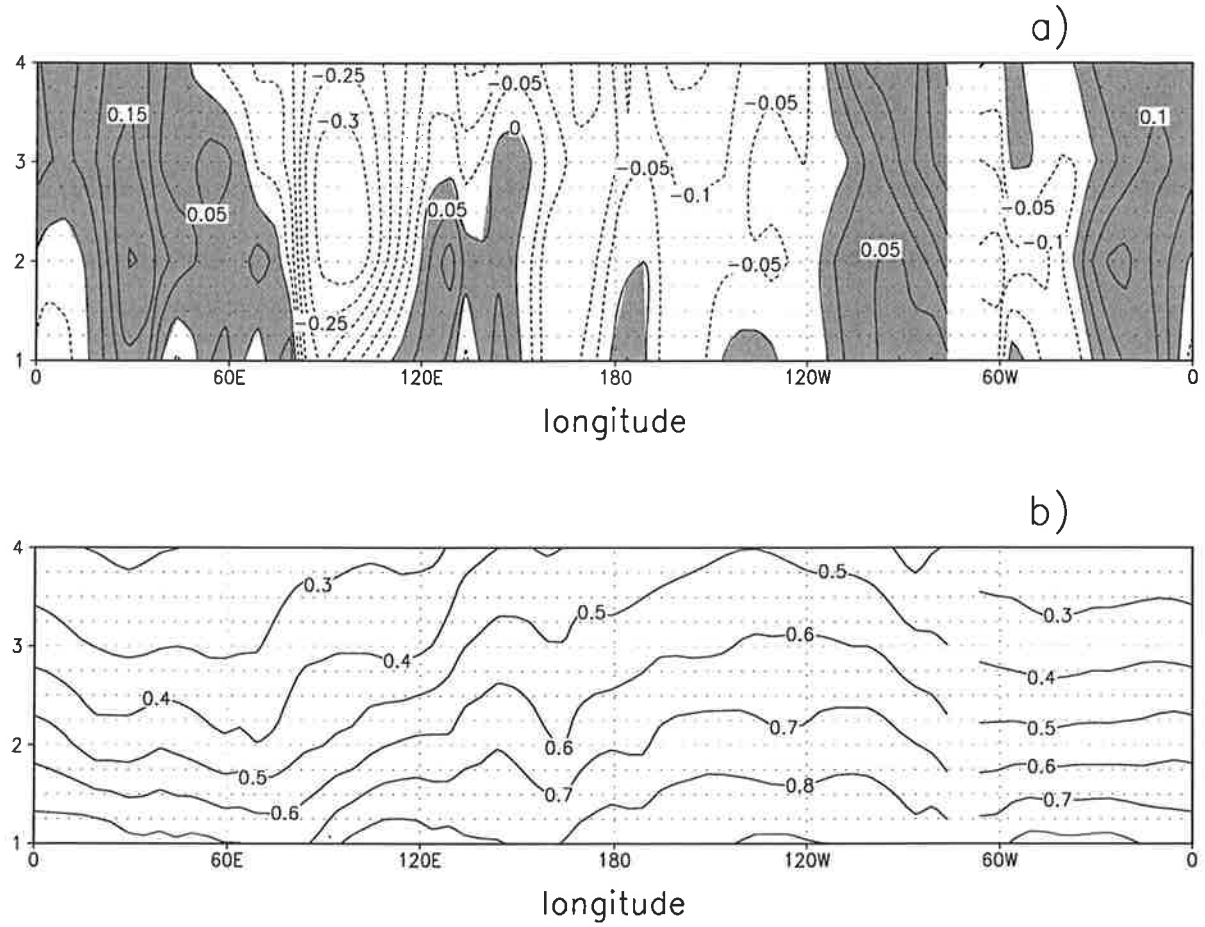

Figure 9. Asymmetry (a) and spread (b) derived from the cross correlation matrix of SSS at 51° South. Contour interval is 0.05 for asymmetry (a) and 0.1 for spread (b). Negative isolines are dashed. Areas with positive values are shaded in (a). For definitions see text.

upper levels which tend to propagate eastward along the ACC at the mean current velocity. The amplitude of the anomalies is at maximum in the Pacific sector of the ACC and almost negligible in the Indian Ocean. The mode was identified by means of a POP analysis of sea surface salinities for which it explains up to 35% of the total variance. POP analysis and inspection of the lagged correlation matrix of the raw data reveal that the anomalies are enforced or generated southwest of Australia. Accordingly, they are advected through the Pacific sector of the ACC and are decaying in the East Pacific and after having passed through Drake Passage. The time scale of the variability was found to be 6 years.

The wavenumber-frequency spectra of the raw salinity and temperature data of the LSG experiment correspond to those of a stochastic climate model with linear feedback and advection in which the ocean acts primarily as integrator of the short-term atmospheric fluctuations and transfers them into a red response signal. The wavenumber-frequency spectra of the random components which were superimposed on the climatological fluxes of heat, momentum, and freshwater were found to be dominated by wavenumbers one, two and three. Given that the linear feedback is small compared to the product of mean current velocity $\bar{u}$ and dominant wavenumber k_0 of the forcing, the time scale of the ocean variability in the stochastic model is given by $(k_0\bar{u})^{-1}$ which in our case yields roughly 6 years for $k_0 = 3$ and $\bar{u} = 4.5$ cms^{-1}, the average speed of the ACC in the LSG model. For e.g. a given dominant wavenumber four in the atmospheric forcing the time scale would be decreased at given ACC speed or, the other way around, an average speed of the ACC of roughly 3.4 cms^{-1} would be required to maintain the time scale of the variability. Thus, the large-scale spatial coherence of the atmospheric forcing is transferred to the ocean which together with the mean velocity of the ACC determines the time scale of the variability.

There are strong similarities between the Antarctic Circumpolar Wave as described by WP for observations and by CBR for a CGCM and the decadal variability found in the LSG experiment. WP suggested that phase-locked anomalies of SST, SLP and mean meridional wind stress completely circle around the globe, whereas CBR emphasized that the ACW is basically confined to the Pacific sector of the ACC and is much weaker in the Atlantic and the Indian Ocean. In our ocean-only experiment in which atmosphere-ocean feedbacks are completely neglected the amplitude of the mode is at maximum in the Pacific sector of the ACC and almost negligible in the Indian Ocean which coincides with the findings of CBR. Note that, since the spatial characteristics of the atmospheric forcing were found to be important for the temporal and the spatial scale of the oceanic variability, our findings cannot be considered as completely independent of those of CBR: The atmospheric part of their CGCM is almost the same as the one used for the AMIP simulation (Arpe et al., 1993) from which the stochastic forcing of the LSG experiment in the present study was derived.

Both WP and CBR noted phase-locked anomalies of atmospheric and oceanic variables which propagate eastward along the ACC and concluded that the ACW reflects a mode of the coupled atmosphere-ocean system. In contrast, we found that even a stochastic atmospheric forc-

ing is able to generate an organized oceanic response which shows noticeable similarities with the variability described by WP and CBR. Consequently, phase-locking between atmosphere and ocean and ocean-atmosphere feedbacks seem not to be prerequisites for such variability to occur. One might even speculate that the atmosphere responds with phase-locked signals to ocean anomalies whose time scale is eventually determined by the ocean itself. However, the resolution of the ocean model used in the present study is relatively coarse compared to the spatial scale of fronts, eddies, and jet-streams in the ACC which are considered to be crucial for its dynamics. As a result, the average speed of the ACC is only roughly 4-5 cms^{-1} in our model compared to the 6-8 cms^{-1} obtained by WP from observations. Consequently, the time scale of the variability is increased in the LSG model.

In order to investigate the physical mechanisms of the decadal variability in the ACC, CBR forced a simple one-dimensional ocean heat budget model for the ACC with a standing wave given by a spatially fixed wavenumber three and an oscillation period of 4 years. They were able to excite SST anomalies with a zonal wavenumber three distribution which propagate eastward along the ACC. However, no explanation was given where the 4-year period of the atmospheric fluctuations might come from. By using a similar simple model, we showed in the present study that irregular atmospheric fluctuations in time are sufficient to excite propagating signals in the SST or SSS. With a spatially fixed zonal wavenumber three pattern we were able to reconstruct basic features of the variability in the ACC such as the spatial scale of the ocean response or the propagation of the anomalies at the mean velocity of the ACC. With a combination of spatially fixed wavenumber three and two patterns we were also able to reconstruct the zonal modifications of the amplitude of the decadal variability. The notion of the importance of the spatial scale of the atmospheric forcing for the time scale of the oceanic variability is somewhat supported by the analyses of Mo and White (1985) and of Xu et al. (1990) who showed that a preference of the atmosphere to attribute energy to the zonal wavenumber three in the standing part of the spectrum in mid-latitudes of the southern hemisphere does exist.

For the derivation of the stochastic climate model for decadal ACC variability we assumed that the source terms of the transport equations can be expanded with respect to temperature and salinity (linear feedback). Furthermore, we assumed that the linear feedback is independent of space. However, the results of the cross-correlation analysis in section 3.4 suggest that the internal memory of the system is not constant but varies with longitude. This indicates that

ocean feedback processes on a local scale might very well be involved in building up the decadal variability in the ACC. However, since basic features of the variability could be reconstructed with an even simpler model, such local feedback processes were not explicitly taken into account in the present study. We suggest that the combined effects of anomaly advection by the mean ocean circulation, integration of random short-term atmospheric weather fluctuations and some linear ocean feedback account for a considerable fraction of the observed variability.

Acknowledgements.

We are thankful for the valuable comments provided by Dr. Eduardo Zorita and Dr. Reiner Schnur in numerous and stimulating discussions and in carefully reading the manuscript.

References

Arakawa, A., and V.R. Lamb, Computational design of the basic processes of the UCLA general circulation model, *Methods Comput. Phys.*, 17, 173-265, 1977.

Arpe, K., L. Bengtsson, and E. Roeckner, The impact of sea surface temperature anomalies on the variability of the atmospheric circulation in the ECHAM3 model, in *Research Activities in atmospheric and oceanic modelling*, edited G. Boer, pp. 7.18-7.20, WMO-Report No. 18, Geneva, 1993.

Christoph, M., T.P. Barnett, and E. Roeckner, The Antarctic circumpolar wave in a coupled ocean atmosphere GCM, *MPI-Report,* 235, 28pp., Max-Planck-Institut für Meteorologie, Hamburg, 1997.

Frankignoul, C., and R. W. Reynolds, Testing a dynamical model for mid-latitude sea surface temperature anomalies, *J. Phys. Oceanogr.*, 13, 1131-1145, 1983.

Hasselmann, K., Stochastic climate models. Part I, Theory, *Tellus*, 28, 473-485, 1976.

Hellerman, S., and M. Rosenstein, Normal monthly wind stress data over the world ocean with error estimates, *J. Phys. Oceanogr.*, 13, 1093-1104, 1983.

Jacobs, G.A. and J.L Mitchell, Ocean circulation variations associated with the Antarctic, *Geophys. Res. Lett.*, 23, 2947-2950, 1996.

Lemke, P., E.W. Trinkl, and K. Hasselmann, Stochastic dynamic analysis of polar sea ice variability, *J. Phys. Oceanogr.*, 10, 2100-2120, 1980.

Levitus, S., Climatological atlas of the world ocean, *NOAA Prof. Pap.*, 13, U.S. Govt. Print. Office, Washington D.C., 1982.

Maier-Reimer, E., U. Mikolajewicz, and K. Hasselmann, Mean circulation of the Hamburg LSG OGCM and its sensitivity to the thermohaline surface forcing, *J. Phys. Oceanogr.*, 23, 731-757, 1993.

Mikolajewicz, U., and E. Maier-Reimer, Mixed boundary conditions in ocean general circulation models and their influence on the stability of the models conveyor belt, *J. Geophys. Res.*, 99, 22633-22644, 1994.

Mo, K.C., and G.H. White, Teleconnections in the Southern Hemisphere, *Mon. Wea. Rev.*, 113, 22-37, 1985.

Murphy, E.J., A. Clarke, C. Symon, and J. Priddle, Temporal variations in Antarctic sea-ice: analysis of a long term fast-ice record from the South Orkney Islands, *Deep Sea Res.*, 42, 1045-1062, 1995.

Peterson, R.G., and W. B. White, Propagation of Pacific ENSO signals throughout the Southern Hemisphere via the Antarctic Circumpolar Current, *Submitted to Nature*, 1996.

Pratt, R.W., The interpretation of space time spectral quantities, *J. Atmos. Sci.*, 32, 1283-1300, 1976.

Press, W.H., S.A. Teukolsky, W.T. Vetterling, and B. P. Flannery, *Numerical recipes. The art of scientific computing.* Cambridge University Press, Cambridge, 436-448, 1992.

Schmitz, W.J.Jr., On the interbasin scale thermohaline circulation, *Rev. Geophys.*, 33, 151-173, 1995.

Schnur, R., G. Schmitz, N. Grieger, and H. von Storch, Normal modes of the atmosphere as estimated by Principal Oscillation Patterns and derived from quasi-geostrophic theory, *J. Atmos. Sci.*, 50, 2386-2400, 1993.

Schnur, R., Baroklin instabile Welle der Atmosphäre: Empisrisch abgeleitete Moden im Vergleich zu quasi-geostrophischer Theorie, Ph.D. thesis, University of Hamburg, Hamburg, 70pp., 1993. [Available from Max-Planck-Institut für Meteorologie, Bundesstraße 55, D-20146 Hamburg, Gemany]

UNESCO, Algorithms for computation of fundamental properties of sea water, *UNESCO Technical Papers in Marine Sci.*, 44, Paris, 1983.

von Storch, H., G. Bürger, R. Schnur, and J.S. von Storch, Principal Oscillation Patterns: A Review, *J. Clim.*, 8, 377-400, 1995.